Basal forebrain GABAergic innervation of olfactory bulb periglomerular interneurons

Running title: inhibitory inputs of olfactory bulb interneurons

Alvaro Sanz Diez[1], Marion Najac[2] and Didier De Saint Jan[1]

[1]Institut des Neurosciences Cellulaires et Intégratives, Centre National de la Recherche Scientifique, Unité Propre de Recherche 3212, Université de Strasbourg, 67084 Strasbourg, France, [2]Department of Neurobiology, Northwestern University, Evanston, Illinois 60208.

Corresponding authors:
desaintjan@inci-cnrs.unistra.fr
Institut des Neurosciences Cellulaires et Intégratives, CNRS UPR 3212, 5 rue Blaise Pascal, 67084 Strasbourg, France

Authors contributions: ASD and DDSJ did the experiments, MN contributed essential preliminary data, DDSJ wrote the paper. All authors edited the manuscript.

Abstract: 219 words; introduction: 582 words; discussion: 1380 words

Key points summary

- Basal forebrain long-range projections to the olfactory bulb are important for olfactory sensitivity and odor discrimination.
- Using optogenetics, we confirm that basal forebrain afferents mediate IPSCs on granule and deep short axon cells. We also show that they selectively innervate specific subtypes of periglomerular (PG) cells.
- The three different subtypes of type 2 PG cells receive GABAergic IPSCs from the basal forebrain but not from other PG cells.
- Type 1 PG cells, in contrast, do not receive inputs from the basal forebrain but do receive inhibition from other PG cells.
- These results bring new light on the complexity and specificity of glomerular inhibitory circuits, as well as on their modulation by the basal forebrain.

Abstract

Olfactory bulb circuits are dominated by multiple inhibitory pathways that finely tune the activity of mitral and tufted cells, the principal neurons, and regulate odor discrimination. Granule cells mediate interglomerular lateral inhibition between mitral and tufted cells lateral dendrites whereas diverse subtypes of periglomerular (PG) cells mediate intraglomerular lateral inhibition between their apical dendrites. Deep short axon cells form broad intrabulbar inhibitory circuits that regulate both populations of interneurons. Little is known about the extrabulbar GABAergic circuits that control the activity of these various interneurons. We examined this question using patch-clamp recordings and optogenetics in olfactory bulb slices from transgenic mice. We show that axonal projections emanating from diverse basal forebrain GABAergic neurons densely project in all layers of the olfactory bulb. These long-range GABAergic projections provide a prominent synaptic input on granule and short axon cells in deep layers as well as on selective subtypes of PG cells. Specifically, three different subclasses of type 2 PG cells receive robust and target-specific basal forebrain inputs but have little local interactions with other PG cells. In contrast, type 1 PG cells are not innervated by basal forebrain fibers but do interact with other PG cells. Thus, attention-regulated basal forebrain inputs regulate inhibition in all layers of the olfactory bulb with a previously overlooked synaptic complexity that further defines interneuron subclasses.

Introduction

Olfactory bulb circuits transform the spatially organized sensory input carried by olfactory sensory neurons (OSNs) into a temporal code in mitral and tufted cells, the principal neurons that relay the information to cortical areas. In the olfactory bulb, inhibitory interneurons vastly outnumber mitral and tufted cells and form several inhibitory circuits that shape the output of principal neurons. In addition, thousands of newborn inhibitory neurons are integrated every postnatal day in the pre-existing olfactory bulb network. Inhibition thus plays fundamental roles in early olfactory bulb processing, as demonstrated by multiple evidence *in vivo* (Abraham *et al.*, 2010;

68 Lepousez & Lledo, 2013; Fukunaga *et al.*, 2014; Gschwend *et al.*, 2015; Economo *et al.*,
69 2016).

70 Olfactory bulb interneurons are diverse but three large classes dominate: granule
71 cells, periglomerular (PG) cells and short-axon (SA) cells. Granule cells, the most
72 abundant type, form reciprocal dendrodendritic synapses with the lateral dendrites of
73 mitral and tufted cells in the external plexiform layer. PG interneurons, in contrast,
74 interact with the apical dendrites of mitral and tufted cells within the glomeruli. PG
75 cells usually project within a single glomerulus, often lack an axon and are functionally,
76 morphologically and chemically highly diverse (McQuiston & Katz, 2001; Kosaka &
77 Kosaka, 2007; Panzanelli *et al.*, 2007; Parrish-Aungst *et al.*, 2007; Whitman & Greer,
78 2007; Kosaka & Kosaka, 2011; Najac *et al.*, 2015; Benito *et al.*, 2018). They have been
79 classified in two broad functional classes depending on their excitatory inputs. The
80 majority are so-called type 2 PG cells and receive excitatory inputs exclusively from the
81 dendrites of mitral and tufted cells whereas type 1 PG cells receive direct excitatory
82 inputs from OSNs (Kosaka & Kosaka, 2007; Shao *et al.*, 2009). This simple classification,
83 however, does not fully reflect the functional heterogeneity of PG cells (McQuiston &
84 Katz, 2001; Najac *et al.*, 2015; Benito *et al.*, 2018). Finally, SA cells with soma located in
85 the glomerular layer (superficial SA cells) or in the granule cell layer (deep or dSA cells),
86 unlike what their name suggest, possess long ramifying axons that form broad
87 intrabulbar connections. Diverse subtypes of deep SA cells mediate a widespread
88 interneuron-specific inhibition (Eyre *et al.*, 2008; Boyd *et al.*, 2012; Burton *et al.*, 2017)
89 whereas superficial SA cells inhibit external tufted cells (Liu *et al.*, 2013; Whitesell *et*
90 *al.*, 2013).

91 Granule, PG and SA cells receive GABAergic synaptic inputs but only a few studies
92 have investigated their origin. These inputs could arise from local intrabulbar
93 interactions or from extrabulbar afferences. The olfactory bulb receives centrifugal
94 GABAergic projections from the basal forebrain, particularly from the horizontal limb
95 of the Diagonal Band of Broca (HDB) and from the magnocellular preoptic nucleus
96 (MCPO) (Zaborszky *et al.*, 1986; Gracia-Llanes *et al.*, 2010; Niedworok *et al.*, 2012).
97 These long-range projections make functional connections with granule (Nunez-Parra
98 *et al.*, 2013) and dSA cells (Case *et al.*, 2017) and their pharmacological inactivation
99 impairs olfactory sensitivity and odor discrimination (Nunez-Parra *et al.*, 2013). Little is

100 known, however, about their connections in the glomerular layer. We here examined
101 the targets of centrifugal basal forebrain axons in olfactory bulb interneurons. We used
102 patch-clamp recording and light activation of channelrhodopsin-2 (ChR2) targeted to
103 basal forebrain GABAergic neurons in acute slices from dlx5/6-Cre transgenic mice. We
104 specifically focused on PG cells and examined whether GABAergic inputs differ in
105 distinct subclasses of PG cells. The results indicate that long-range basal forebrain
106 GABAergic projections broadly regulate olfactory bulb circuits and innervate specific
107 PG cell subtypes with a previously unexpected level of synaptic complexity.
108

109 **Materials and Methods**

110 *Animals*. All experimental procedures were approved by the French Ministry and the
111 local ethic committee for animal experimentation (C.R.E.M.E.A.S). We used dlx5/6-Cre
112 female mice that express the Cre recombinase under the control of the regulatory
113 sequences of the dlx5 and dlx6 genes (Monory *et al.*, 2006), and Kv3.1-EYFP mice of
114 either sex that express the enhanced yellow fluorescent protein (EYFP) under the
115 control of the Kv3.1 K^+ channel promoter (Metzger *et al.*, 2002).

116 *Slice preparation.* 3 weeks to 3 month-old mice were killed by decapitation and the
117 olfactory bulbs rapidly removed in ice-cold oxygenated (95% O2-5% CO2) solution
118 containing (in mM): 83 NaCl, 26.2 NaHCO3, 1 NaH2PO4, 2.5 KCl, 3.3 MgSO4, 0.5 CaCl2,
119 70 sucrose and 22 D-glucose (pH 7.3, osmolarity 300 mOsm/l). Horizontal olfactory
120 bulb slices (300 µm) were cut using a Microm HM 650V vibratome (Microm, Germany)
121 in the same solution; incubated for 30-40 minutes at 34°C; stored at room
122 temperature in a regular artificial cerebrospinal fluid (ACSF) until use. ACSF contained
123 (in mM): 125 NaCl, 25 NaHCO3, 2.5 KCl, 1.25 NaH2PO4, 1 MgCl2, 2 CaCl2 and 25 D-
124 glucose and was continuously bubbled with 95% O2-5% CO2.

125 *Electrophysiological recordings.* Experiments were conducted at 32-34°C under an
126 upright microscope (SliceScope, Scientifica, Uckfield, UK) with differential interference
127 contrast (DIC) optics. Whole-cell recordings were made with glass pipettes (3-6 MΩ)
128 filled with a K-gluconate-based internal solution containing (in mM): 135 K-gluconate,
129 2 $MgCl_2$, 0.025 $CaCl_2$, 1 EGTA, 4 Na-ATP, 0.5 Na-GTP, 10 Hepes (pH 7.3, 280 mOsm).
130 Atto 594 (10 µM, Sigma) was added to the internal solution in order to visualize the
131 cell morphology. Loose cell-attached recordings (15-100 MΩ seal resistance) were

132 made with pipettes filled with ACSF. OSN axons bundles projecting inside a given
133 glomerulus were electrically stimulated using a theta pipette filled with ACSF as
134 previously described (Najac *et al.*, 2015). The electrical stimulus (100 µs) was delivered
135 using a Digitimer DS3 (Digitimer, Welwyn Garden City, UK). Optical stimulation was
136 done through a blue (490 nm) CoolLED pE 100 (CoolLED Ltd., Andover, UK) directed
137 through the 40X objective of the microscope. Recordings were acquired with a
138 multiclamp 700B amplifier (Molecular Devices, Sunnyvale, CA), low-passed filtered at
139 2-4 kHz and digitized at 10 kHz using the AxoGraph X software (Axograph Scientific). In
140 current-clamp recordings, a constant hyperpolarizing current was injected in order to
141 maintain the cell at a potential of -60/-70 mV. In voltage-clamp recordings, access
142 resistance (Ra<30 MΩ for PG, granule and deep SA cells) was not compensated.
143 Voltages indicated in the paper were corrected for the junction potential (-15 mV).
144 *Drugs.* 6-nitro-7-sulfamoylbenzo[f]quinoxaline-2,3-dione (NBQX), D-2-Amino-5-
145 phosphonopentanoic acid (D-AP5), 2-(3-carboxypropyl)-3-amino-6-(4
146 methoxyphenyl)pyridazinium bromide (GBZ) were purchased from Abcam
147 Biochemicals.
148 *Stereotaxic viral injections*. 3-6 weeks old dlx5/6-cre female mice were anesthetized
149 with intraperitoneal injection of ketamine (20%), acepromazine (6%) and
150 medetomidine (11.8%) mix (100µl/10g) and placed in a stereotaxic apparatus. Mice
151 were craneotomized and a volume of 200-500 nl of
152 AAV9.EF1a.DIO.hChR2(H134R).eYFP.WPRE.hGH or AAV9.EF1a.DIO.eYFP.WPRE.hGH
153 (University of Pennsylvania Viral Vector Core) was stereotaxically injected with a
154 Pneumatic Picopump PV 820, at 0.2 mm AP, -1.6 mm ML and -5.6 mm DV from
155 bregma. After surgery, mice were injected with Metacam 100 (meloxicam) (5%)
156 (100µl/10g), Antisedan (atipamezol) (2.5%) (100µl/10g), rehydrated with 1 ml of NaCl
157 0.9% and placed under a heating lamp. Mice recovered during 3-4 weeks after
158 injection before anatomical or physiological experiments.
159 *Analysis.* EPSCs, IPSCs or photocurrent amplitudes were measured as the peak of an
160 average response computed from multiple sweeps. The decay of light-evoked IPSCs
161 was most often best fitted with a double exponential with time t=0 at the peak of the
162 current. Time constant values indicated in the text are weighted decay time constants
163 calculated using the following equation: $\tau_w = (\tau_1 A_1 + \tau_2 A_2)/(A_1 + A_2)$ where τ_1 and τ_2 are

164 the fast and slow decay time constants and A_1 and A_2 are the equivalent amplitude
165 weighting factors. To estimate the duration of an OSN-evoked plurisynaptic excitatory
166 response, individual EPSCs with amplitude >5 pA were automatically detected by the
167 Axograph X software using a sliding template function. PSTH (peri stimulus time
168 histograms) representing the cumulative number of EPSCs per 20 ms bin across several
169 consecutive sweeps were then constructed. The decaying phase of these histograms
170 was fitted with a single or with two exponentials to provide a time constant of the
171 OSN-evoked response duration.
172
173 *Statistics.* Data are expressed as mean ± SD. We used the Student's *t*-test to assess the
174 statistical difference between paired sets of data with normal distribution, the non-
175 parametric Wilcoxon-Mann-Whitney rank sum test to assess the statistical difference
176 between unpaired sets of data, the Kruskal-Wallis test for data sets with more than
177 two variables and p-values are reported.
178
179 *Immunohistochemistry.* Adult mice (1-3 months) were deeply anesthetized with
180 intraperitoneal injection of xylazine (6.3%) and ketamine (25%) and intracardially
181 perfused with 4% paraformaldehyde (PFA). Brains were removed and kept in 4% PFA
182 overnight. Slices were cut (50 µm thick) with a vibratome (Leica VT 1000S). Blocking
183 steps were performed using a PBS solution containing 2% BSA or 5% goat serum and
184 0.3% Triton X-100 during 2h. Sections were incubated overnight at 4°C with primary
185 antibodies: goat anti-choline acetyltransferase (ChAT; 1:500; Millipore Cat# AB144P,
186 RRID:AB_2079751), mouse anti-parvalbumin (PV; 1:1000; Sigma-Aldrich Cat# P3088,
187 RRID:AB_477329), rabbit anti-calretinin (CR; 1:1000; Swant Cat# 7697,
188 RRID:AB_2721226) or mouse anti-calbindin D28K (CB; 1:1000; Sigma-Aldrich Cat#
189 C9848, RRID:AB_476894). After three washes in PBS, sections were incubated 2 hours
190 at room temperature with the corresponding secondary antibodies —Alexa fluor 633
191 conjugated goat anti-rabbit (1:500; ThermoFisher A-21070) and Alexa fluor 633
192 conjugated goat anti-mouse (1:500; ThermoFisher A-21050) or Alexa fluor 647
193 conjugated donkey anti-goat (1:200; ThermoFisher A-21447). After three washes,
194 sections were mounted in Prolong Diamond Antifade Mountant (ThermoFisher).
195 Images were taken using a Leica TCS SP5 II confocal microscope or an Axio Imager M2

196 for mosaic images. Immunostained and EYFP-expressing cells were manually counted
197 using Cell counter plug-in on Fiji software.
198
199
200 **Results**
201 **Selective expression of ChR2 in GABAergic neurons of the HDB**
202 We used an optogenetic approach to map the functional synaptic connections of
203 basal forebrain GABAergic neurons onto olfactory bulb interneurons. We injected an
204 adeno-associated virus encoding a Cre-inducible ChR2-EYFP fusion protein in the basal
205 forebrain of dlx5/6-Cre mice, a transgenic line that expresses the Cre recombinase
206 exclusively in GABAergic neurons in the forebrain (Monory *et al.*, 2006)(Figure 1A).
207 These injections produced a dense EYFP labeling of fibers in the olfactory bulb. Labeled
208 fibers were particularly abundant in the granule cell layer and in the glomerular layer
209 of the bulb, similarly to a previous study using a Cre-dependent viral approach in the
210 GAD65-Cre mouse (Nunez-Parra *et al.*, 2013). In the basal forebrain, expression of
211 ChR2-EYFP was intense around the injection site but was limited to the membrane,
212 making cell bodies difficult to distinguish. Hence, we injected the same virus expressing
213 cytosolic EYFP to verify the specificity of the recombination in GABAergic neurons
214 (Figure 1B, n=5 mice). EYFP was expressed in cell bodies of various sizes around the
215 injection site. Some of these cells also expressed the calcium-binding proteins
216 calretinin (CR, n=122 cells counted), calbindin (CB, n=54) or parvalbumin (PV, n=25),
217 three classical markers of GABAergic neurons that label non-overlapping neural
218 populations in the basal forebrain (Zaborszky *et al.*, 2005). EYFP also colocalized with
219 choline acetyltransferase (ChAT), the enzyme for acetylcholine synthesis, in about 1/3
220 of the ChAT(+) neurons counted (n=63/190 cells), consistent with the idea that
221 cholinergic neurons in the basal forebrain are also GABAergic (Saunders *et al.*, 2015).
222 We then tested the synaptic connections made by ChR2-expressing basal
223 forebrain axons in the olfactory bulb using whole-cell voltage-clamp recordings in
224 olfactory bulb slices. Consistent with previous reports (Nunez-Parra *et al.*, 2013; Case
225 *et al.*, 2017), activating ChR2-expressing basal forebrain axons with brief (1-10 ms)
226 flashes of blue light evoked outward inhibitory postsynaptic currents (IPSCs) in granule
227 cells (n=9/11, range 67-464 pA, mean 161±124 pA at Vh=0 mV, Figure 2A) and dSA cells

228 (n=10/10, range 30-681 pA, mean 379±170 pA at Vh between -15 and -35 mV, Figure
229 2B). In 2 of the 10 dSA cells tested, the response had two components that reversed at
230 different potentials. At Vh=-70 mV, the response was biphasic with an outward
231 component that was blocked by the $GABA_A$ receptor antagonist gabazine (GBZ, 5 µM),
232 and an inward component that persisted in the presence of GBZ. These dual responses
233 are similar to those mediated by VGLUT3(+) basal forebrain neurons that release both
234 GABA and acetylcholine onto a specific subtype of dSA cells with axonal projections in
235 the glomerular layer (Case et al. 2017). They were therefore not further studied.
236 Most PG cells tested also responded to the photostimulation with an IPSC
237 (n=63/82, range 6-849 pA, mean 220±201 pA at Vh=0 mV, Figure 2C). Light-evoked
238 IPSCs sometime displayed multiple peaks or deflections during the rising phase
239 indicating that they resulted from summating IPSCs (not shown). However, responses
240 were unaffected by the presence of the AMPA and NMDA receptor antagonists, NBQX
241 and D-AP5 respectively, demonstrating that they were monosynaptic (n=14 PG cells,
242 Figure 2C). Thus, IPSCs recorded in ACSF or in NBQX/D-AP5 were pooled for analysis.
243 Evoked IPSCs were totally abolished by GBZ (n=10 PG cells, Figure 2C), had a single
244 component that reversed at the expected equilibrium potential for chloride (ECl=-88
245 mV in our recording conditions, n=12 PG cells, Figure 2D). Light-evoked IPSCs had a
246 uniformly fast time course in dSA cells (mean decay time constant 11.7±5.9 ms) and in
247 granule cells (29±6.4 ms). In contrast, the duration of light-evoked IPSCs was highly
248 variable in PG cells (decay time constant range 6-254 ms, mean 46.9±56.1 ms)(Figure
249 2E). However, light-responsive PG cells had diverse firing and synaptic properties,
250 suggesting that the variable time course of their basal forebrain input may reflect PG
251 cell diversity. To further validate this possibility, we classified the recorded PG cells in
252 distinct subtypes based on their membrane properties and OSN-evoked synaptic
253 responses and then examined their GABAergic synaptic inputs.
254
255 **Type 1 PG cells are not innervated by basal forebrain afferences**
256 Type 1 PG cells constituted 11% of the PG cells recorded in dlx5/6;ChR2-EYFP mice
257 (9/82). These neurons fired multiple action potentials in response to a membrane
258 supra-threshold step depolarization. Their discharge was regular (n=2), irregular (as in
259 Figure 3A, n=3) or a burst of spikes (n=3). They responded to the electrical stimulation

260 of OSNs with a fast onset monosynaptic EPSC (mean latency 1.59±0.25 ms)(Figure 3B
261 and 3E). The onset of this EPSC varied little across trials even at low intensities of
262 stimulation (jitter 0.09±0.04 ms) whereas the response of type 2 PG cells had a longer
263 onset latency (>2 ms) that increased and became more variable with stimulations of
264 lower intensity (Figure 3E). OSN stimulation also induced IPSCs in 8/9 type 1 PG cells
265 voltage-clamped at Vh=0 mV, i.e. around the reversal potential for excitation (Figure
266 3B, 3D). This inhibitory response was composed of multiple asynchronous IPSCs,
267 consistent with a plurisynaptic input generated within the glomerular network by
268 other PG cells activated by the stimulation. However, none of the 9 type 1 PG cells
269 tested responded to the photo stimulation of the basal forebrain fibers (Figure 3C).
270 Thus, type 1 PG cells receive inhibitory inputs from neighboring PG cells but not from
271 the basal forebrain.
272
273 **Different classes of type 2 PG cells receive basal forebrain inputs with target-specific**
274 **properties**
275 Type 2 PG cells were largely predominant in our recordings in dlx5/6;ChR2-EYFP mice
276 (n=68/82, 83%) and all PG cells responding to the flash of blue light with an IPSC were
277 type 2 PG cells. We classified these type 2 PG cells in three subclasses, based on their
278 membrane properties and OSN-evoked synaptic responses, as followed:
279
280 **1. CR-expressing type 2 PG cells**
281 The most numerous cell type (n=29, 35%) showed the distinctive membrane and
282 synaptic properties of CR-expressing PG cells (Fogli Iseppe *et al.*, 2016; Benito *et al.*,
283 2018), consistent with the predominance of this subtype within the entire population.
284 These cells fired at most a single action potential or a spikelet and were passively
285 depolarized by a suprathreshold current step (Figure 4A). In addition, these PG cells
286 received few spontaneous EPSCs (not shown), had small OSN-evoked excitatory inputs
287 (Figure 4B, 4C) and usually large electrical membrane resistance (Figure 4D). OSN
288 stimulations evoked small IPSCs or no IPSC at all in these cells clamped at Vh=0mV
289 (Figure 4B, 4C) as previously reported in genetically-identified CR-expressing PG cells
290 (Benito *et al.*, 2018). In contrast, photo stimulation of basal forebrain fibers evoked a
291 GBZ-sensitive IPSC in 27/29 cells (Figure 4E). These light-evoked IPSCs were often large

292 (average amplitude 294±196 pA, range 6-741 pA) and always fast (average decay time
293 constant 11.9±3.6 ms, range 6-21 ms)(Figure 4E). Thus, a fast basal forebrain-mediated
294 GABAergic input is another attribute of CR-expressing PG cells.
295
296 **2. CB-like type 2 PG cells with short OSN-evoked excitatory responses**
297 The second group of type 2 PG cells (n=18, 22%) included cells that responded to OSN
298 stimulations with a short burst of asynchronous EPSCs (average duration 33±25 ms,
299 range 12-100 ms)(Figure 5B). We have previously shown that cells with this type of
300 response are heterogeneous in terms of firing properties but include CB-expressing PG
301 cells (Najac *et al.*, 2015). Cells classified in this group were thus called CB-like PG cells.
302 The majority (n=10) responded to a depolarizing current step with a single spike
303 preceding a plateau potential, as in the example shown in Figure 5A. However, some
304 cells had a regular firing (n=3) and others responded with a burst of action potentials
305 (n=3). Photo stimulation of basal forebrain fibers evoked an IPSC in 13 of these 18 CB-
306 like cells (Figure 5D). Light-evoked responses had a mean amplitude of 140±101 pA
307 (range 24-324 pA) and a decay time constant ranging from 6.7 to 53.8 ms (mean
308 27±14.2 ms)(Figure 5D), significantly slower than in CR-like PG cells (p=0.0027,
309 Wilcoxon test). In contrast, OSN stimulation did not evoke IPSCs (Figure 5B, 5C),
310 suggesting that these cells are not connected to other PG cells.
311 To confirm the absence of connections with other PG cells, we used the Kv3.1-EYFP
312 reporter mouse. A population of type 2 PG cells with short OSN-evoked responses is
313 labeled in this mouse, including CB-expressing cells (Najac *et al.*, 2015). In these
314 experiments, we recorded the whole-cell voltage-clamp response of EYFP(+) PG cells
315 while simultaneously monitoring in loose cell-attached the discharge of a control PG
316 cell projecting into the same glomerulus (either EYFP(+), n=4, or EYFP(-), n=5, Figure
317 5F). OSN stimulations that efficiently drove the firing of the control PG cell induced a
318 robust excitatory response in EYFP(+) PG cells clamped at Vh=-75 mV. This stimulation,
319 however, did not evoke any IPSC when cells were clamped at Vh=0mV (n=9). In a
320 subset of experiments, increasing the stimulation intensity by a factor of 10 also failed
321 to evoke IPSCs (n=6). In contrast, an electrical stimulation in the glomerular layer at
322 >200 µm away from the recorded PG cell evoked a reliable GBZ-sensitive IPSC in
323 EYFP(+) PG cells (n=16, average amplitude 87±48 pA at Vh=0 mV; decay time constant:

324 30±13 ms, range 7.7-53.6 ms) that persisted in the presence of NBQX and D-AP5 (not
325 shown). Our results suggest that this monosynaptic IPSC is mediated by basal forebrain
326 axons ramifying in the glomerular layer, although the possibility that dSA cells also
327 innervate these PG cells cannot be excluded. Thus, CB-like type 2 PG cells responding
328 to the stimulation of OSNs with a short excitatory response do not interact locally with
329 other PG cells but do receive a prominent GABAergic input from the basal forebrain.
330
331 **3. Type 2 PG cells with long-lasting OSN-evoked excitatory responses**
332 The third group of type 2 PG cells (n=18, 22%) is composed of cells that responded to
333 OSN stimulations with a long-lasting barrage of EPSCs, often lasting several hundreds
334 of milliseconds (range 0.1 to >3s, average 792±757 ms)(Figure 6B). All these cells had a
335 regular firing upon injection of a depolarizing step, indicating that this population is
336 quite homogeneous (Figure 6A). Moreover, 17/18 cells in this group responded to the
337 photo stimulation of the basal forebrain axons with a prolonged IPSC (IPSC amplitude
338 193±247 pA, range 11-850 pA; average decay time constant 116±63 ms, range 40-254
339 ms, $p<0.0001$ for comparison with both CR-like and CB-like PG cells, Wilcoxon
340 test)(Figure 6D). These basal forebrain-mediated IPSCs were much larger than the
341 OSN-evoked slow IPSCs that were eventually observed in 6/11 PG cells (Figure 6C).
342 Thus, long-lasting basal forebrain-mediated IPSCs are found in a specific subclass of
343 regularly firing PG cells that responds to an OSN input with a remarkably prolonged
344 barrage of EPSCs.
345 Finally, 10% of the recorded PG cells (n=8), that either had an incomplete
346 characterization or functional properties that did not fit in any of the 4 previously
347 defined subgroups, could not be classified. 6 of these cells responded to the photo
348 stimulation with an IPSC.
349
350 **Diversity of basal forebrain afference**
351 Our data so far indicate that the time course of the basal forebrain synaptic inputs
352 depends on the PG cell subtype they target. To start gaining insight into whether these
353 distinct postsynaptic PG neurons are contacted by different presynaptic fibers, we
354 compared the short-term plasticity at these synapses. We applied a train of 5 blue light
355 pulses at 20 Hz. This photo stimulation evoked IPSCs that depressed at different

356 degrees in the three subclasses of type 2 PG cells as quantified by the paired-pulse
357 ratio of the second IPSC amplitude relative to the first (Kruskal-Wallis test, H=11.38,
358 p=0.0034)(Figure 7). In particular, the paired-pulse depression in CR-like PG cells
359 (0.73±0.13, n=11) was less pronounced than in CB-like PG cells (0.47±0.16, n=8,
360 p=0.0008, Wilcoxon test) and than in PG cells with long-lasting OSN-evoked responses
361 (0.56±0.16, n=8, p=0.020, Wilcoxon test). The paired-pulse ratio was not different in
362 these two last groups (p=0.38, Wilcoxon test) but failures of transmission were
363 frequent in CB-like PG cells (seen in 5/8 cells, Figure 7B) whereas they were never
364 observed in PG cells with long-lasting OSN-evoked responses. Together, these data
365 provide evidence that basal forebrain inputs may be mediated by specific afferent
366 fibers on each subclass of olfactory bulb PG cells.
367
368 **Discussion**
369 Most efforts in understanding the function of inhibition in the olfactory bulb have
370 focused on the local activation mechanisms of the diverse interneuron populations and
371 on the impact of their activity in shaping the olfactory bulb output. In comparison,
372 GABAergic circuits that control the activity of olfactory bulb interneurons have
373 received little attention. We show here that long-range GABAergic projections from
374 the basal forebrain make prominent and specific connections on most classes of
375 interneurons in the olfactory bulb with a previously unsuspected level of synaptic
376 specificity. These data provide additional criteria for PG cells classification and
377 emphasize that each PG cell subtype belong to a specific synaptic circuit, an important
378 step towards understanding the functional implications of their diversity. They also
379 reinforce the idea that the basal forebrain is a major modulator of olfactory bulb
380 circuits whose influence is still partially understood.
381
382 **Basal forebrain projections to the olfactory bulb**
383 The basal forebrain contains several nuclei without clear delineations that
384 innervate the cerebral cortex, limbic areas, hippocampus, thalamic structures and the
385 olfactory bulb with cholinergic and GABAergic projections. Centrifugal projections to
386 the olfactory bulb originate principally from the HDB and MCPO. Cholinergic axons are
387 found essentially in the glomerular layer and in the internal plexiform layer of the bulb

388 and, moderately, in the granule cell layer (Macrides *et al.*, 1981; Zaborszky *et al.*, 1986;
389 Salcedo *et al.*, 2011; Case *et al.*, 2017; Hamamoto *et al.*, 2017). GABAergic projections
390 are even more massive and innervate all layers of the bulb (Zaborszky *et al.*, 1986;
391 Gracia-Llanes *et al.*, 2010; Niedworok *et al.*, 2012; Nunez-Parra *et al.*, 2013).
392 Cholinergic and GABAergic neurons are not clearly segregated in the basal forebrain
393 (Zaborszky *et al.*, 1986), interact between each other (Yang *et al.*, 2014) and nearly all
394 cholinergic neurons express the molecular machinery to co-transmit GABA (Saunders
395 *et al.*, 2015). These two centrifugal pathways are thus intimately coupled and attempts
396 to evaluate their influence independently have to be interpreted with caution.
397 Nevertheless, several reports demonstrate that ACh modulates diverse bulbar neurons
398 at different timescales and via multiple pre- and postsynaptic muscarinic and nicotinic
399 receptors (Castillo *et al.*, 1999; Ghatpande & Gelperin, 2009; Devore *et al.*, 2014; Liu *et*
400 *al.*, 2015; Smith *et al.*, 2015). Optogenetic manipulation of basal forebrain cholinergic
401 neurons modulates odor detection, discrimination and olfactory learning (Ma & Luo,
402 2012; Rothermel *et al.*, 2014). Our results indicate that basal forebrain GABAergic
403 neurons also have multiple targets in the bulb. Not surprisingly, pharmacological
404 inactivation of HDB/MCPO GABAergic neurons using a DREADD/CNO paradigm impairs
405 olfactory sensitivity and odor discrimination (Nunez-Parra *et al.*, 2013). The basal
406 forebrain therefore stands as a major modulator of olfactory bulb circuits but
407 understanding its global impact on olfactory bulb processing may first require a careful
408 investigation of its action on each targeted neuronal population.
409

410 **GABAergic synaptic connections discriminate different classes of PG cells**

411 We closely examined the GABAergic inputs of olfactory bulb PG cells. The results
412 demonstrate that GABAergic connections are an additional criterion that helps
413 classifying diverse PG cell subtypes. First, type 1 and type 2 PG cells can be
414 distinguished on the basis of their inhibitory input. Basal forebrain fibers contact
415 different subtypes of type 2 PG cells but not type 1 PG cells. Moreover, type 2 PG cells
416 have little synaptic interactions with other PG cells whereas type 1 PG cells do.
417 Previous studies revealed that GABAergic lateral interactions between PG cells
418 projecting within the same glomerulus are mediated, at least in part, by GABA spillover

419 (Smith & Jahr, 2002; Murphy *et al.*, 2005). Our results further suggest that more
420 conventional PG-PG cells synaptic interactions may be restricted to type 1 PG cells.

421 Second, we show that basal forebrain axons produce IPSCs with distinct time
422 courses and short term plasticities in three subgroups of type 2 PG cells that also differ
423 on the basis of their OSN-evoked excitatory response and firing properties. IPSCs with
424 diverse durations likely reflect different subunit compositions of postsynaptic $GABA_A$
425 receptors. For instance, a subpopulation of PG cells that does not overlap with CB- and
426 CR-expressing PG cells selectively expresses the alpha5 subunit (Panzanelli *et al.*,
427 2007). Expression of this subunit correlates in some neurons with slow IPSCs (Pangratz-
428 Fuehrer *et al.*, 2016) suggesting that the alpha5 subunit may be a molecular marker of
429 the type 2 PG cells with regular firing and a long-lasting OSN-evoked excitatory
430 response.

431 We limited our characterization to a subset of electrophysiological properties
432 that, in our recording conditions, could be unambiguously established. A full
433 characterization that correlates membrane and synaptic properties with morphological
434 and molecular features would most likely define additional subclasses of type 2 PG
435 cells. PG cells with short-lasting OSN-evoked excitatory responses, for instance, have
436 heterogeneous firing patterns and include CB-expressing and CB-lacking PG cells (Najac
437 *et al.*, 2015). However, those are challenging experiments in mice lacking a genetically-
438 encoded marker that labels a specific subpopulation.

439 Postsynaptic $GABA_A$ receptors with different kinetics contribute in shaping short
440 term depression. However, our analysis of paired pulse ratio and failure rate suggest
441 that the different degrees at which basal forebrain IPSCs depressed in PG cells also
442 reflect presynaptic diversity. Thus, distinct subsets of chemically-defined basal
443 forebrain GABAergic neurons may have spatially defined projections in the olfactory
444 bulb and control specific bulbar interneuron populations. Consistent with this
445 hypothesis, a recent report demonstrates that a specific subset of GABA/ACh basal
446 forebrain neurons preferentially projects in the internal plexiform layer of the olfactory
447 bulb where it selectively connects with one specific subtype of dSA cells (Case *et al.*,
448 2017). Thus, addressing the synaptic complexity of basal forebrain GABAergic inputs in
449 the olfactory bulb may necessitate the use of transgenic mice allowing the visualization
450 and manipulation of selective genetically-identified population of neurons.

451

452 **Role of basal forebrain GABAergic afferents in olfactory bulb odor processing**

453 We show the connections of basal forebrain GABA fibers with PG and granule cells
454 that, together, constitute the main populations of interneurons directly regulating the
455 activity of olfactory bulb output neurons. Deep SA cells also provide inhibitory input on
456 PG and granule cells (Eyre *et al.*, 2008; Burton *et al.*, 2017) and are themselves
457 modulated by basal forebrain inputs. This diversity of olfactory bulb interneurons
458 under the control of basal forebrain fibers makes it challenging to predict the global
459 functional implications of this GABAergic innervation on the olfactory bulb output. In
460 the simplest way, inhibition of olfactory bulb interneurons may induce a disinhibition
461 of mitral and tufted cells and thus facilitate the olfactory bulb output. However, GABA
462 may be excitatory on some PG cells (Parsa *et al.*, 2015). Moreover, co-transmission of
463 GABA and ACh on, at least, some interneurons (Case *et al.*, 2017), also complicates this
464 view. Moreover, as olfactory bulb processing is fundamentally rhythmic and tightly
465 coupled to respiration, the physiological impact of basal forebrain centrifugal inputs
466 may depend on their temporal dynamics along a respiration cycle. A synchronized
467 activity of these centrifugal afferents may reset the activity of olfactory bulb
468 interneurons before a new respiration cycle. But how synchronized are they? Recent
469 data indicate that some non-cholinergic neurons in the HDB have their activity
470 correlated with attention whereas the activity of cholinergic neurons is correlated with
471 primary reinforcers and outcome expectations (Hangya *et al.*, 2015). Centrifugal inputs
472 from the basal forebrain could therefore contextually modulate the olfactory bulb
473 activity as a function of the internal state.

474 Interestingly, basal forebrain GABAergic fibers and axonal feedback from the
475 olfactory cortex target the same populations of interneurons in the bulb. Thus, axons
476 from pyramidal cells of the piriform cortex or the anterior olfactory nucleus directly
477 excite olfactory bulb interneurons and facilitate mitral cell inhibition (Boyd *et al.*, 2012;
478 Markopoulos *et al.*, 2012), i.e. the exact opposite of what HDB GABAergic fibers might
479 do. Pyramidal cells of the olfactory cortex innervate HDB neurons as well (Paolini &
480 McKenzie, 1997; Linster & Hasselmo, 2000; Do *et al.*, 2016). Centrifugal afferents from
481 the basal forebrain could have complex dynamics, similar as cortical feedback that
482 exerts spatially diffuse, temporally complex and non-uniform actions on olfactory bulb

483 interneurons in response to odors (Boyd *et al.*, 2015; Otazu *et al.*, 2015). Thus, the net
484 impact of cortical feedback and basal forebrain fiber inputs on olfactory bulb
485 interneurons, balancing or opposite actions, may depend on their relative timing in
486 different behavioral context.
487

488 **Acknowledgements**

489 This work was supported by the Centre National pour la Recherche Scientifique, the
490 Université de Strasbourg and the Agence Nationale pour la Recherche (Grant ANR-12-
491 JSV4-006-01). ASD was funded by a fellowship from the Ministère de la Recherche and
492 by a fellowship from the Fonds Paul Mandel pour les Recherches en Neuroscience. We
493 thank Ipek Yalcin (Institut des Neurosciences Cellulaires et Intégratives, Strasbourg)
494 and Claire Gaveriaux-Ruff (Institut de Génétique et de Biologie Moléculaire et
495 Cellulaire, Strasbourg) for the kind gift of the dlx5/6-Cre mice and Thomas Knöpfel
496 (Imperial College, London) for the kind gift of the Kv3.1-EYFP mice. We thank Sophie
497 Reibel-Foisset and the animal facility Chronobiotron (UMS 3415 Centre National pour
498 la Recherche Scientifique and Université de Strasbourg), the Plateforme Imagerie In
499 Vitro-Neuropôle-Strasbourg, and Aline Huber for their technical assistance. We thank
500 Jean Christophe Cassel (Laboratoire de Neurosciences Cognitives et Adaptatives,
501 Strasbourg) Nuria Benito, Philippe Isope, Matilde Cordero-Erausquin, Bernard Poulain,
502 and members of the lab for their constructive comments throughout the project.
503

504 **References**

505 Abraham NM, Egger V, Shimshek DR, Renden R, Fukunaga I, Sprengel R, Seeburg PH, Klugmann
506 M, Margrie TW, Schaefer AT & Kuner T. (2010). Synaptic inhibition in the olfactory bulb
507 accelerates odor discrimination in mice. *Neuron* **65,** 399-411.
508

509 Benito N, Gaborieau E, Sanz Diez A, Kosar S, Foucault L, Raineteau O & De Saint Jan D. (2018).
510 A pool of postnatally-generated interneurons persists in an immature stage in the olfactory
511 bulb. *J Neurosci*.in press.
512

513 Boyd AM, Kato HK, Komiyama T & Isaacson JS. (2015). Broadcasting of cortical activity to the
514 olfactory bulb. *Cell Rep* **10,** 1032-1039.
515

516 Boyd AM, Sturgill JF, Poo C & Isaacson JS. (2012). Cortical feedback control of olfactory bulb
517 circuits. *Neuron* **76,** 1161-1174.
518

519 Burton SD, LaRocca G, Liu A, Cheetham CE & Urban NN. (2017). Olfactory Bulb Deep Short-
520 Axon Cells Mediate Widespread Inhibition of Tufted Cell Apical Dendrites. *J Neurosci* **37,** 1117-
521 1138.
522
523 Case DT, Burton SD, Gedeon JY, Williams SG, Urban NN & Seal RP. (2017). Layer- and cell type-
524 selective co-transmission by a basal forebrain cholinergic projection to the olfactory bulb. *Nat*
525 *Commun* **8,** 652.
526
527 Castillo PE, Carleton A, Vincent JD & Lledo PM. (1999). Multiple and opposing roles of
528 cholinergic transmission in the main olfactory bulb. *J Neurosci* **19,** 9180-9191.
529
530 Devore S, de Almeida L & Linster C. (2014). Distinct roles of bulbar muscarinic and nicotinic
531 receptors in olfactory discrimination learning. *J Neurosci* **34,** 11244-11260.
532
533 Do JP, Xu M, Lee SH, Chang WC, Zhang S, Chung S, Yung TJ, Fan JL, Miyamichi K, Luo L & Dan Y.
534 (2016). Cell type-specific long-range connections of basal forebrain circuit. *Elife* **5**.
535
536 Economo MN, Hansen KR & Wachowiak M. (2016). Control of Mitral/Tufted Cell Output by
537 Selective Inhibition among Olfactory Bulb Glomeruli. *Neuron* **91,** 397-411.
538
539 Eyre MD, Antal M & Nusser Z. (2008). Distinct deep short-axon cell subtypes of the main
540 olfactory bulb provide novel intrabulbar and extrabulbar GABAergic connections. *J Neurosci*
541 **28,** 8217-8229.
542
543 Fogli Iseppe A, Pignatelli A & Belluzzi O. (2016). Calretinin-Periglomerular Interneurons in Mice
544 Olfactory Bulb: Cells of Few Words. *Front Cell Neurosci* **10,** 231.
545
546 Fukunaga I, Herb JT, Kollo M, Boyden ES & Schaefer AT. (2014). Independent control of gamma
547 and theta activity by distinct interneuron networks in the olfactory bulb. *Nat Neurosci* **17,**
548 1208-1216.
549
550 Ghatpande AS & Gelperin A. (2009). Presynaptic muscarinic receptors enhance glutamate
551 release at the mitral/tufted to granule cell dendrodendritic synapse in the rat main olfactory
552 bulb. *J Neurophysiol* **101,** 2052-2061.
553

554 Gracia-Llanes FJ, Crespo C, Blasco-Ibanez JM, Nacher J, Varea E, Rovira-Esteban L & Martinez-
555 Guijarro FJ. (2010). GABAergic basal forebrain afferents innervate selectively GABAergic
556 targets in the main olfactory bulb. *Neuroscience* **170,** 913-922.
557
558 Gschwend O, Abraham NM, Lagier S, Begnaud F, Rodriguez I & Carleton A. (2015). Neuronal
559 pattern separation in the olfactory bulb improves odor discrimination learning. *Nat Neurosci*
560 **18,** 1474-1482.
561
562 Hamamoto M, Kiyokage E, Sohn J, Hioki H, Harada T & Toida K. (2017). Structural basis for
563 cholinergic regulation of neural circuits in the mouse olfactory bulb. *J Comp Neurol* **525,** 574-
564 591.
565
566 Hangya B, Ranade SP, Lorenc M & Kepecs A. (2015). Central Cholinergic Neurons Are Rapidly
567 Recruited by Reinforcement Feedback. *Cell* **162,** 1155-1168.
568
569 Kosaka K & Kosaka T. (2007). Chemical properties of type 1 and type 2 periglomerular cells in
570 the mouse olfactory bulb are different from those in the rat olfactory bulb. *Brain Res* **1167,** 42-
571 55.
572
573 Kosaka T & Kosaka K. (2011). "Interneurons" in the olfactory bulb revisited. *Neurosci Res* **69,**
574 93-99.
575
576 Lepousez G & Lledo PM. (2013). Odor discrimination requires proper olfactory fast oscillations
577 in awake mice. *Neuron* **80,** 1010-1024.
578
579 Linster C & Hasselmo ME. (2000). Neural activity in the horizontal limb of the diagonal band of
580 broca can be modulated by electrical stimulation of the olfactory bulb and cortex in rats.
581 *Neurosci Lett* **282,** 157-160.
582
583 Liu S, Plachez C, Shao Z, Puche A & Shipley MT. (2013). Olfactory bulb short axon cell release of
584 GABA and dopamine produces a temporally biphasic inhibition-excitation response in external
585 tufted cells. *J Neurosci* **33,** 2916-2926.
586

587 Liu S, Shao Z, Puche A, Wachowiak M, Rothermel M & Shipley MT. (2015). Muscarinic
588 receptors modulate dendrodendritic inhibitory synapses to sculpt glomerular output. *J*
589 *Neurosci* **35,** 5680-5692.
590
591 Ma M & Luo M. (2012). Optogenetic activation of basal forebrain cholinergic neurons
592 modulates neuronal excitability and sensory responses in the main olfactory bulb. *J Neurosci*
593 **32,** 10105-10116.
594
595 Macrides F, Davis BJ, Youngs WM, Nadi NS & Margolis FL. (1981). Cholinergic and
596 catecholaminergic afferents to the olfactory bulb in the hamster: a neuroanatomical,
597 biochemical, and histochemical investigation. *J Comp Neurol* **203,** 495-514.
598
599 Markopoulos F, Rokni D, Gire DH & Murthy VN. (2012). Functional properties of cortical
600 feedback projections to the olfactory bulb. *Neuron* **76,** 1175-1188.
601
602 McQuiston AR & Katz LC. (2001). Electrophysiology of interneurons in the glomerular layer of
603 the rat olfactory bulb. *J Neurophysiol* **86,** 1899-1907.
604
605 Metzger F, Repunte-Canonigo V, Matsushita S, Akemann W, Diez-Garcia J, Ho CS, Iwasato T,
606 Grandes P, Itohara S, Joho RH & Knopfel T. (2002). Transgenic mice expressing a pH and Cl-
607 sensing yellow-fluorescent protein under the control of a potassium channel promoter. *Eur J*
608 *Neurosci* **15,** 40-50.
609
610 Monory K, Massa F, Egertova M, Eder M, Blaudzun H, Westenbroek R, Kelsch W, Jacob W,
611 Marsch R, Ekker M, Long J, Rubenstein JL, Goebbels S, Nave KA, During M, Klugmann M, Wolfel
612 B, Dodt HU, Zieglgansberger W, Wotjak CT, Mackie K, Elphick MR, Marsicano G & Lutz B.
613 (2006). The endocannabinoid system controls key epileptogenic circuits in the hippocampus.
614 *Neuron* **51,** 455-466.
615
616 Murphy GJ, Darcy DP & Isaacson JS. (2005). Intraglomerular inhibition: signaling mechanisms of
617 an olfactory microcircuit. *Nat Neurosci* **8,** 354-364.
618
619 Najac M, Sanz Diez A, Kumar A, Benito N, Charpak S & De Saint Jan D. (2015). Intraglomerular
620 lateral inhibition promotes spike timing variability in principal neurons of the olfactory bulb. *J*
621 *Neurosci* **35,** 4319-4331.

622
623 Niedworok CJ, Schwarz I, Ledderose J, Giese G, Conzelmann KK & Schwarz MK. (2012). Charting
624 monosynaptic connectivity maps by two-color light-sheet fluorescence microscopy. *Cell Rep* **2,**
625 1375-1386.
626
627 Nunez-Parra A, Maurer RK, Krahe K, Smith RS & Araneda RC. (2013). Disruption of centrifugal
628 inhibition to olfactory bulb granule cells impairs olfactory discrimination. *Proc Natl Acad Sci U S*
629 *A* **110,** 14777-14782.
630
631 Otazu GH, Chae H, Davis MB & Albeanu DF. (2015). Cortical Feedback Decorrelates Olfactory
632 Bulb Output in Awake Mice. *Neuron* **86,** 1461-1477.
633
634 Pangratz-Fuehrer S, Sieghart W, Rudolph U, Parada I & Huguenard JR. (2016). Early postnatal
635 switch in GABAA receptor alpha-subunits in the reticular thalamic nucleus. *J Neurophysiol* **115,**
636 1183-1195.
637
638 Panzanelli P, Fritschy JM, Yanagawa Y, Obata K & Sassoe-Pognetto M. (2007). GABAergic
639 phenotype of periglomerular cells in the rodent olfactory bulb. *J Comp Neurol* **502,** 990-1002.
640
641 Paolini AG & McKenzie JS. (1997). Intracellular recording of magnocellular preoptic neuron
642 responses to olfactory brain. *Neuroscience* **78,** 229-242.
643
644 Parrish-Aungst S, Shipley MT, Erdelyi F, Szabo G & Puche AC. (2007). Quantitative analysis of
645 neuronal diversity in the mouse olfactory bulb. *J Comp Neurol* **501,** 825-836.
646
647 Parsa PV, D'Souza RD & Vijayaraghavan S. (2015). Signaling between periglomerular cells
648 reveals a bimodal role for GABA in modulating glomerular microcircuitry in the olfactory bulb.
649 *Proc Natl Acad Sci U S A* **112,** 9478-9483.
650
651 Rothermel M, Carey RM, Puche A, Shipley MT & Wachowiak M. (2014). Cholinergic inputs from
652 Basal forebrain add an excitatory bias to odor coding in the olfactory bulb. *J Neurosci* **34,** 4654-
653 4664.
654

655 Salcedo E, Tran T, Ly X, Lopez R, Barbica C, Restrepo D & Vijayaraghavan S. (2011). Activity-
656 dependent changes in cholinergic innervation of the mouse olfactory bulb. *PLoS One* **6,**
657 e25441.
658
659 Saunders A, Granger AJ & Sabatini BL. (2015). Corelease of acetylcholine and GABA from
660 cholinergic forebrain neurons. *Elife* **4**.
661
662 Shao Z, Puche AC, Kiyokage E, Szabo G & Shipley MT. (2009). Two GABAergic intraglomerular
663 circuits differentially regulate tonic and phasic presynaptic inhibition of olfactory nerve
664 terminals. *J Neurophysiol* **101,** 1988-2001.
665
666 Smith RS, Hu R, DeSouza A, Eberly CL, Krahe K, Chan W & Araneda RC. (2015). Differential
667 Muscarinic Modulation in the Olfactory Bulb. *J Neurosci* **35,** 10773-10785.
668
669 Smith TC & Jahr CE. (2002). Self-inhibition of olfactory bulb neurons. *Nat Neurosci* **5,** 760-766.
670
671 Whitesell JD, Sorensen KA, Jarvie BC, Hentges ST & Schoppa NE. (2013). Interglomerular lateral
672 inhibition targeted on external tufted cells in the olfactory bulb. *J Neurosci* **33,** 1552-1563.
673
674 Whitman MC & Greer CA. (2007). Adult-generated neurons exhibit diverse developmental
675 fates. *Dev Neurobiol* **67,** 1079-1093.
676
677 Yang C, McKenna JT, Zant JC, Winston S, Basheer R & Brown RE. (2014). Cholinergic neurons
678 excite cortically projecting basal forebrain GABAergic neurons. *J Neurosci* **34,** 2832-2844.
679
680 Zaborszky L, Buhl DL, Pobalashingham S, Bjaalie JG & Nadasdy Z. (2005). Three-dimensional
681 chemoarchitecture of the basal forebrain: spatially specific association of cholinergic and
682 calcium binding protein-containing neurons. *Neuroscience* **136,** 697-713.
683
684 Zaborszky L, Carlsen J, Brashear HR & Heimer L. (1986). Cholinergic and GABAergic afferents to
685 the olfactory bulb in the rat with special emphasis on the projection neurons in the nucleus of
686 the horizontal limb of the diagonal band. *J Comp Neurol* **243,** 488-509.
687
688

689 **Figures and legends**

690

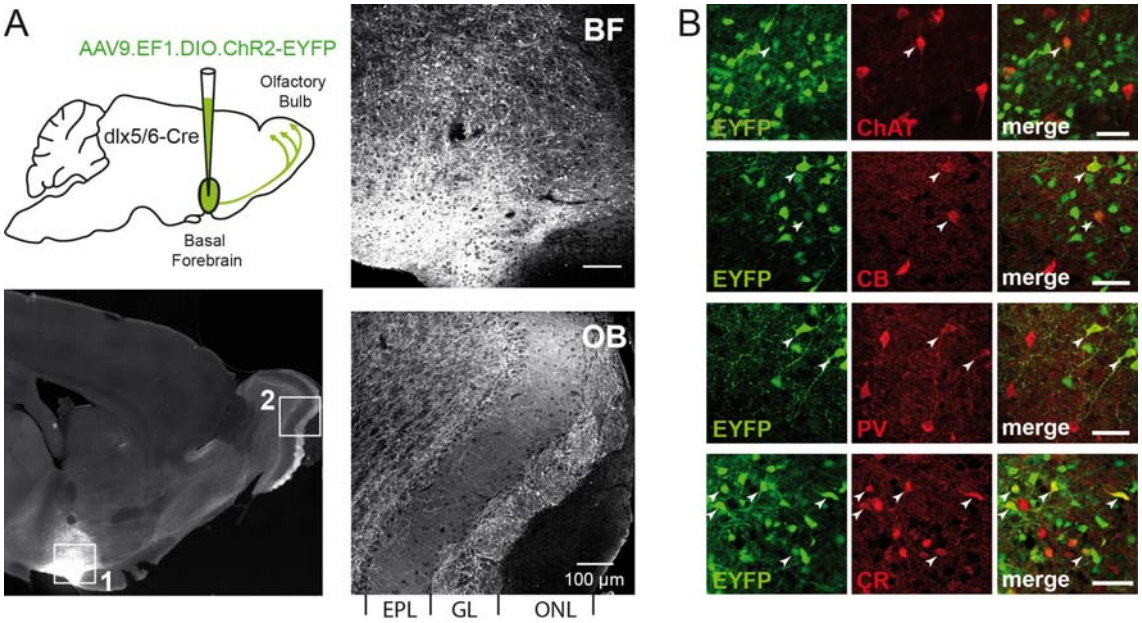

691

692

693 **Figure 1: Conditional expression of ChR2 in various GABAergic neurons of the basal**
694 **forebrain. A,** Stereotaxic injection of a viral construct in the basal forebrain of dlx5/6-
695 Cre mice was used for conditional expression of ChR2-EYFP in GABAergic neurons of
696 the basal forebrain. Bottom left, sagittal section of a brain 4 weeks after the injection.
697 The site of injection (BF, boxed area 1) and the olfactory bulb (OB, boxed area 2) are
698 enlarged in the two other pictures. ONL: olfactory nerve layer, GL: glomerular layer,
699 EPL: external plexiform layer. **B,** EYFP expression in the basal forebrain 4 weeks after
700 injection of the same viral construct encoding cytosolic EYFP. Co-staining of EYFP
701 (green) together with ChAT, CB, PV or CR (red). Some neurons (arrowheads), but not
702 all, co-express the two markers. Scale bars 50 µm.

703

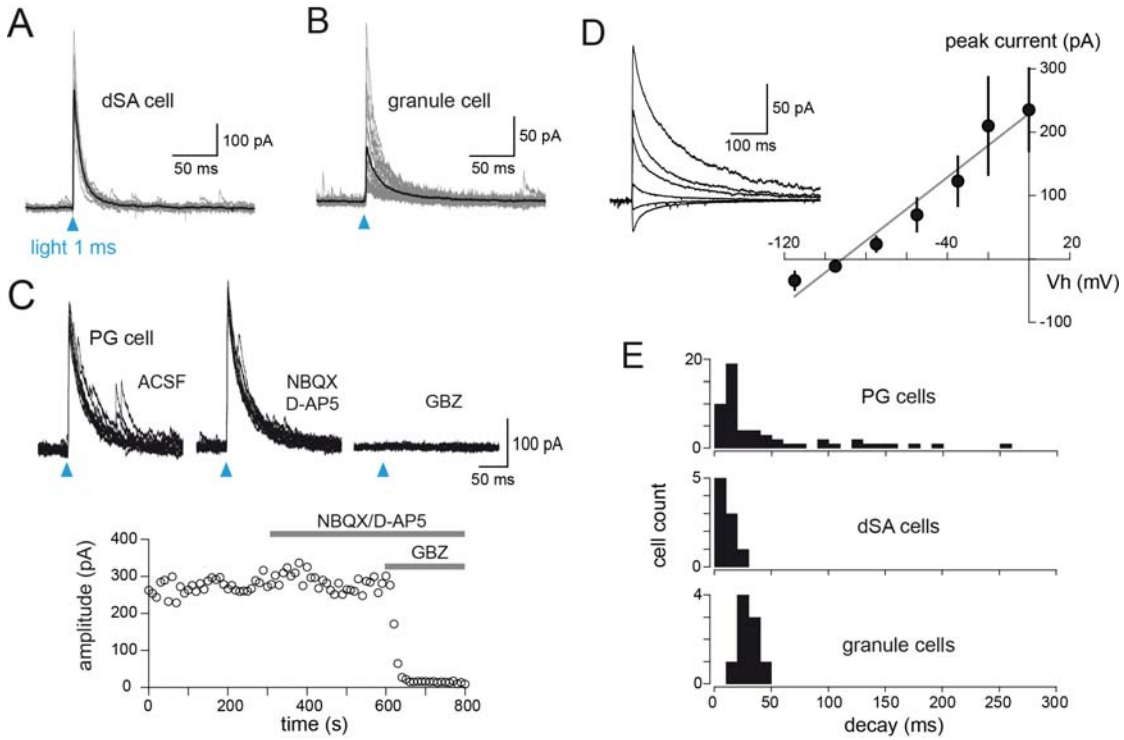

704
705

706 **Figure 2. Synaptic connections of basal forebrain axons with various inhibitory**
707 **interneurons of the olfactory bulb. A,** Light-evoked consecutive ISPCs evoked in a
708 deep SA cell recorded at Vh=-15 mV in the presence of AMPA and NMDA receptor
709 blockers (10 µM NBQX + 50 µM D-AP5). The black trace is the average response. Light
710 stimulation (1 ms) at blue arrow. **B,** Same in a granule cell recorded at Vh=0 mV. **C,**
711 Light-evoked IPSCs elicited in a PG cell (Vh=0mV) in control condition, in the presence
712 of NBQX and D-AP5 and after the addition of gabazine (5 µM, GBZ) to the cocktail.
713 Several traces are superimposed for each condition. The graph shows the amplitude of
714 consecutive responses in these different conditions. **D,** Average current-voltage
715 relationship of the light-evoked IPSC in PG cells (n=12 cells, each plot is an
716 average±sem). Inset, IPSCs from a representative PG cell recorded at different holding
717 potentials. **E,** Decay time constants distribution of light-evoked IPSCs recorded in PG,
718 dSA and granule cells. PG and granule cells were recorded at Vh=0mV, dSA cells at Vh
719 comprised between -35 mV and -15 mV.

720

721

722

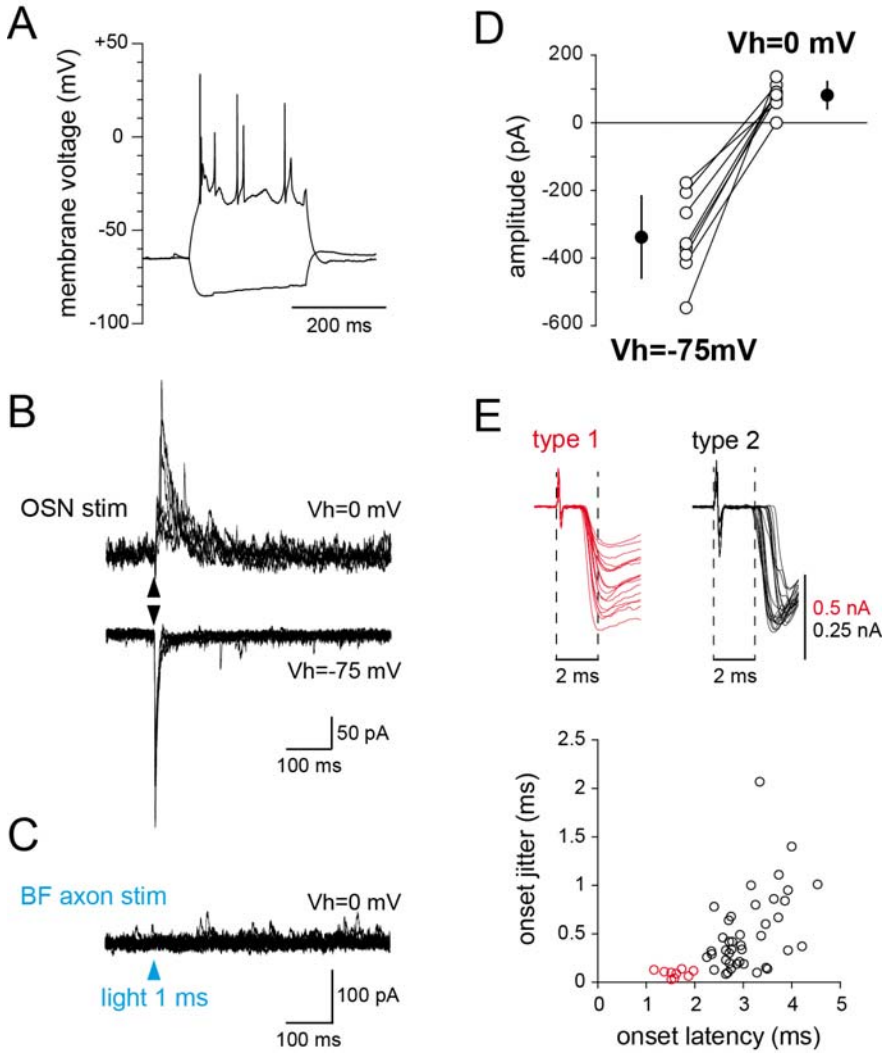

723

724

725 **<u>Figure 3</u>: Type 1 PG cells are not contacted by basal forebrain projections but are**
726 **inhibited by other PG cells.** Membrane properties (**A**), OSN-evoked synaptic responses
727 (**B**) and responses to basal forebrain axons photo stimulation (**C**) of a type 1 PG cell
728 recorded in a dlx5/6;ChR2-EYFP mouse. This cell responded to the stimulation of OSN
729 with an inward fast monosynaptic EPSC at Vh=-75 mV and with outward plurisynaptic
730 IPSCs at Vh=0 mV (**B**). In contrast, light stimulation of basal forebrain fibers did not
731 evoke any response (**C**). Several traces are superimposed in each case. **D,** Summary
732 plots for OSN-evoked synaptic response amplitudes of all type 1 PG cells tested at two
733 holding potentials. **E,** Classification of the recorded PG cells into type 1 and type 2 in
734 dlx5/6;ChR2-EYFP mice. Top, early phase of OSN-evoked EPSCs in a type 1 PG cell (red)
735 and in a type 2 PG cell (black). The type 1 PG cell responded with a short latency EPSC,

736 starting <2ms after the beginning of the stimulation artifact and with little onset
737 variability between trials. In contrast, responses from the type 2 PG cell had a delayed
738 and more variable onset latency. The graph shows the onset latency vs. onset jitter of
739 OSN-evoked responses in PG cells classified as type 1 PG cells (red circles) and in PG
740 cells classified as type 2 PG cells (black circles) in this study.
741

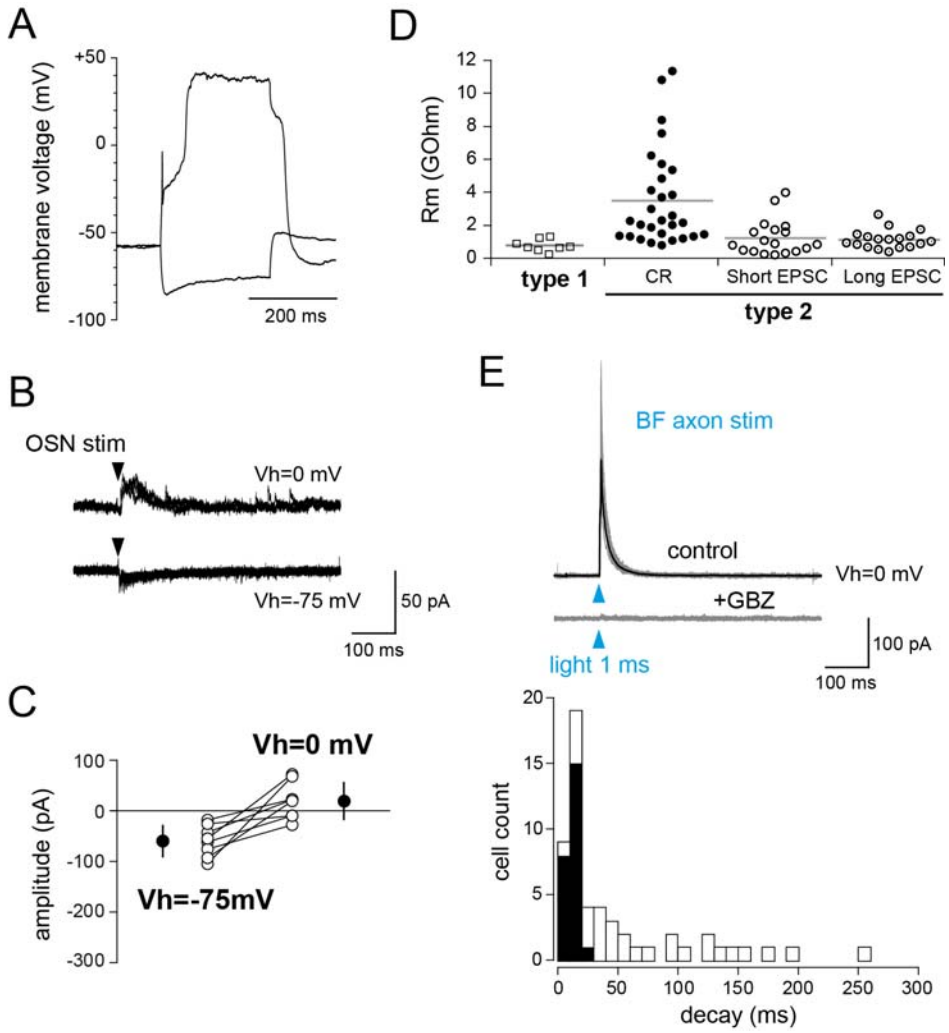

<u>Figure 4</u>: CR-expressing type 2 PG cells receive fast basal forebrain GABAergic inputs. Membrane properties (**A**) and OSN-evoked synaptic responses (**B**) of a typical CR-expressing type 2 PG cell recorded in a dlx5/6;ChR2-EYFP mouse. This cell typically responded to a suprathreshold depolarization with a single spikelet followed by a passive membrane depolarization (**A**) and had small OSN-evoked responses at Vh=-75 mV and at Vh=0 mV (**B**). **C**, summary plots for OSN-evoked synaptic responses recorded at Vh=-75 mV and at Vh=0 mV for cells classified as CR-expressing PG cells. **D**, cells classified as CR-expressing type 2 PG cells also had larger electrical membrane resistances compared to PG cells classified in the other groups (horizontal bars show the averages, $p<0.001$ for comparison with each of the 3 other subgroups, Wilcoxon test). **E,** light stimulation of basal forebrain fibers evoked large and fast GBZ-sensitive

756 IPSCs in CR-expressing PG cells. Traces are from the same cell as in A and B. The
757 average IPSC (black trace) is superimposed on several consecutive responses recorded
758 at Vh=0mV in ACSF. Bottom, distribution histogram of the decay time constants of
759 light-evoked IPSCs in cells classified as CR-expressing PG cells (black bars)
760 superimposed on the distribution histogram for all the recorded PG cells (white bars).
761

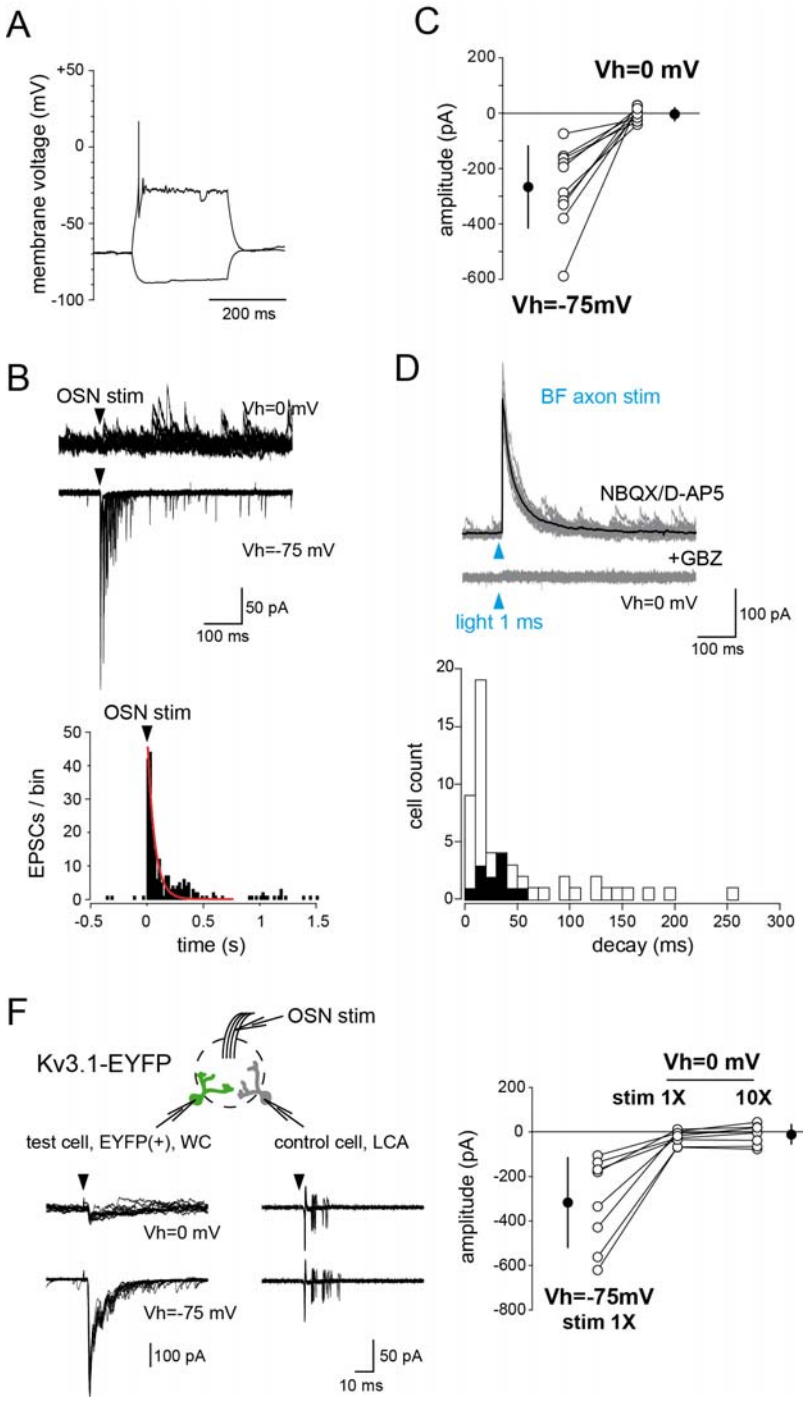

762

763

764 **<u>Figure 5</u>: Type 2 PG cells with short OSN-evoked excitatory response do not interact**
765 **with other PG cells but receive inputs from the basal forebrain.** Membrane properties
766 (**A**) and OSN-evoked synaptic responses (**B**) of a typical type 2 PG cell that responded
767 to the stimulation of the OSN with a short burst of EPSCs in a dlx5/6;ChR2-EYFP mouse.
768 The short (<100 ms) OSN-evoked excitatory response was the main criterion for

769 classifying PG cells in this subclass. The duration of the response was quantified using
770 an exponential fit (red trace, decay time constant 67 ms) of the OSN-evoked PSTH
771 (bottom). **C**, Summary plots (right) for OSN-evoked synaptic responses recorded at
772 Vh=-75 mV and at Vh=0 mV indicate that cells in this group also had no OSN-evoked
773 IPSC. **D**, IPSCs evoked by a light stimulation of the basal forebrain fibers. The average
774 IPSC (black trace) is superimposed on several consecutive responses recorded at
775 Vh=0mV in the presence of NBQX and D-AP5. GBZ abolished the response. Traces are
776 from the same cell as in A and B. Bottom, distribution histogram of the decay time
777 constants of light-evoked IPSCs in PG cells classified in this subclass (black bars)
778 superimposed on the distribution histogram for all the recorded PG cells (white bars).
779 **F**, Paired recording of two PG cells projecting in the same glomerulus in the Kv3.1-EYFP
780 transgenic mouse. The "test" EYFP(+) PG cell was recorded in the whole-cell
781 configuration at Vh=0 mV to monitor IPSCs and at Vh=-75 mV to monitor EPSCs. The
782 "control" PG cell was recorded in the loose cell-attached configuration to monitor its
783 firing. OSNs were stimulated at an intensity inducing the firing of the control PG cell.
784 The summary graph on the right shows that OSN stimulations did not evoke any
785 outward IPSC in the test cell even when the stimulation was increased by a factor of
786 10.
787

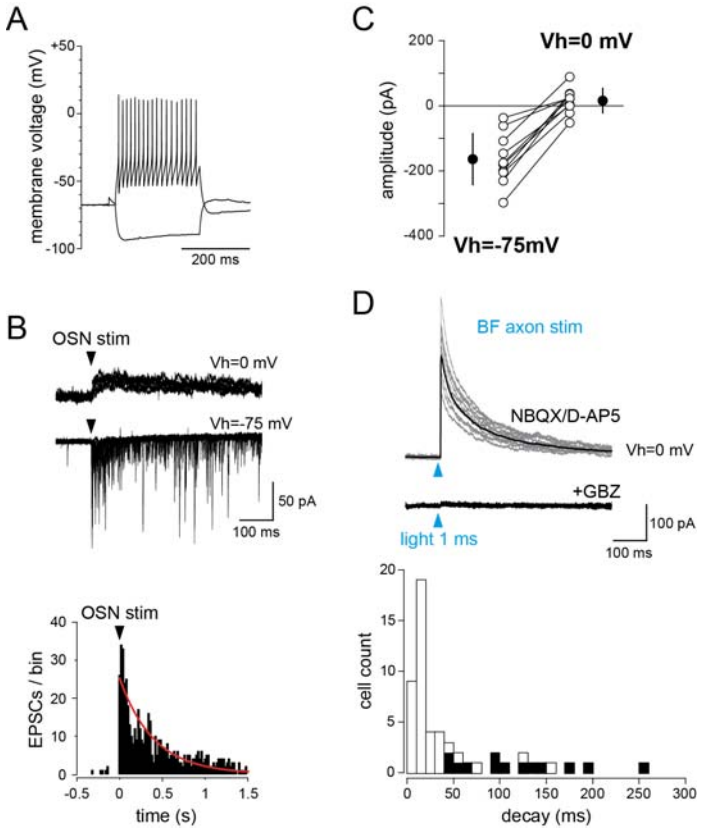

<u>Figure 6</u>: Type 2 PG cells with long-lasting OSN-evoked excitatory response receive slow GABAergic inputs from the basal forebrain. Membrane properties (**A**) and OSN-evoked synaptic responses of a typical type 2 PG cell that responded to the stimulation of the OSN with a long-lasting burst of EPSCs in a dlx5/6;ChR2-EYFP mouse. **A**, Like all the cells included in this group, this PG cell responded to a step depolarization with a regular firing. **B**, OSN-evoked responses recorded at two holding potentials. The PSTH of the excitatory response (bottom) was fitted with an exponential (red trace) with a decay time constant of 396 ms. **C**, Summary plots for OSN-evoked synaptic responses recorded at Vh=-75 mV and at Vh=0 mV for cells included in this group. **D**, IPSCs evoked by a light stimulation of the basal forebrain fibers. The average IPSC (black trace) is superimposed on several consecutive responses recorded at Vh=0mV in the presence of NBQX and D-AP5. GBZ abolished the response. Same cell as in A and B. Bottom, distribution histogram of the decay time constants of light-evoked IPSCs in PG cells classified in this subclass (black bars) superimposed on the distribution histogram for all the recorded PG cells (white bars). Cells included in this group had slow IPSCs.

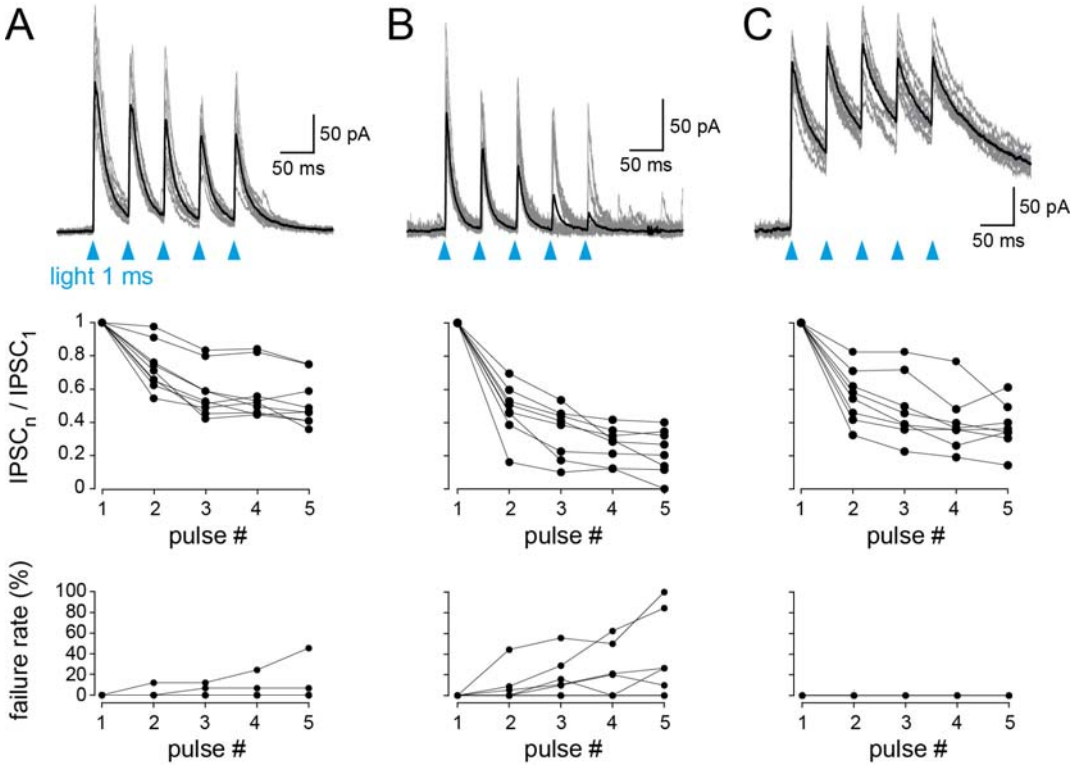

Figure 7 : Basal forebrain GABAergic inputs have different presynaptic properties depending on the postsynaptic PG cell subtype. A-C, Top row, light-evoked IPSCs in three PG cells representative of the three subclasses of type 2 PG cells recorded in dlx5/6;ChR2-EYFP mice (**A**: CR-expressing PG cells; **B**: PG cells with short OSN-evoked excitatory responses and **C**: regularly firing PG cells with long-lasting OSN-evoked responses). Each cell was stimulated with 5 flashes of light at 20 Hz. 10-12 consecutive responses are superimposed for each cell, the black trace is the average response. **Middle row,** amplitudes of the nth light-evoked IPSC relative to the normalized amplitude of the first IPSC recorded in PG cells classified in the 3 subgroups of the corresponding column. Lines connect plots from the same cells. **Bottom row**, failure rate for each of the five consecutive stimuli and for each cell over multiple trials. Failures were never observed in the third group.